This article has been accepted for publication in a future issue of this journal, but has not been fully edited. Content may change prior to final publication. Citation information: DOI 10.1109/ACCESS.2019.2892113, IEEE Access

A novel Smeared Synthesized LFM TC-OLA Radar System: Design and Performance Evaluation

AHMED YOUSSEF, PETER F. DRIESSEN *(Senior Member, IEEE)*, FAYEZ GEBALI *(Life Senior Member, IEEE)*, AND MOA BELAID

***Abstract*—This paper introduces a novel smeared synthesized LFM (SSLFM) time compression overlap-add (TC-OLA) radar system. The new system allows us to control the signal to noise ratio (SNR) level, and, therefore, obtain a higher processing gain compared to the traditional LFM-PC radar systems. In addition, it allows us to control the signal spectrum spreading, making it more immune to noise jamming. The new SSLFM signal is obtained by either multiplying the LFM waveform with a complex unit signal with random phase, or by encoding the time compression (TC) signal with random phase at the transmitter. A denoising processor, placed either before or after the OLA processor, is used to remove the random phase from the SSLFM and forward the resulted LFM signal to the rest of the conventional LFM-PC radar receiver system. The new SSLFM TC-OLA radar system enjoys a better low probability of intercept feature while maintaining the LFM time sidelobe and Doppler tolerance properties. Moreover, the additional modules in the new radar system do not require changing the core LFM radar components. Using TC-OLA and denoising require a synchronization system (SS) to properly recover the LFM signal. We, therefore, offer three synchronization systems (SSs). The performance evaluation of the new radar system shows its superiority over the traditional LFM, the wideband LFM and the TC-OLA-based LFM radars, especially under powerful noise jamming. The synchronization system is implemented and tested experimentally using software-defined radar (SDR).**

***Index Terms*—Communication systems, radar systems, synchronization systems, time compression overlap-add, linear frequency modulation, signal to noise ratio, convolution noise jamming, spread spectrum, software-defined radar.**

I. Introduction

As radars are increasingly facing serious threats from electronic warfare support (ES) interception capabilities and electronic attack (EA), they have to hide their emissions from hostile receivers. Low probability of intercept (LPI) radars use low-power managed waveforms, which are hard to detect without using sophisticated hardware and signal processing algorithms. Many articles are published trying to introduce new LPI waveforms [1–3], especially noise-related ones. The authors of [4, 5] designed a synthesized LFM waveform by combining of random noise waveform and conventional LFM. Their idea is to multiply the conventional LFM signal by a complex noise waveform with a phase factor to control the phase randomness. By increasing the phase factor, the randomness of the obtained signal increases and therefore a higher LPI is achieved. However, the Doppler shift of the moving targets, even the slow ones, cannot be resolved if a large signal phase factor is used. This introduces a trade-off between high LPI and reasonable Doppler tolerance. The authors, therefore, had to use a small phase factor with an optimized matched filter to maintain the estimation accuracy (range and Doppler) with a fair LPI. To obtain high LPI and Doppler tolerance, we propose a new radar system that relies on time compression overlap-add (TC-OLA) technique [6, 7] and allows for large phase factors.

The TC-OLA-based LFM radar introduced in [8, 9], incorporate time compression (TC) and overlap-add (OLA) modules as a pre- and post-processors into an LFM-PC radar. At the transmitter side and using a TC module, the digitally generated LFM signal is divided into overlapping segments. Each segment is transmitted using higher rates to produce non-overlapping segments. At the receiver side, the signal is reconstructed from the segments at the original lower sampling rate using the OLA module and passed to the traditional LFM-PC receiver.

We extend the TC-OLA-based LFM radar by using a synthesized LFM waveform instead. The new radar system obtained requires adding a few modules to harness the power of complex noise waveform with large phase factors. The modules include two Hadamard multipliers, one at the transmitter side to "noise" the LFM signal and produce the synthesized LFM waveform, and the other at the receiver side to denoise the synthesized LFM waveform and convert it back to the traditional LFM. Since the denoising process requires the received signal and the multiplicative complex conjugate of the noise waveform to be fully synchronized, a synchronization module at the receiver side is needed. Because of the LFM signal is noised, scrambled and spread via TC, we qualify our radar system as 'smeared'.

The proposed radar is simulated, evaluated, and then compared with traditional LFM, wideband LFM[1], and TC-OLA based LFM radar systems.

The SSLFM radar enjoys many features, aside from those of TC-OLA-based LFM radar reported in [8], which we enumerate below:

1) Synthesis of new signal with noise-like nature using high phase factor while still possessing LFM features (fair time resolution and high Doppler tolerance).
2) Significant increase of the radar immunity against noise jamming technique compared to traditional LFM, wideband LFM with the same processing gain, and TC-OLA-based LFM radar systems.
3) No change in the radar signal processing blocks, namely matched filter (MF), moving target detector (MTD), and

[1]When the signal bandwidth is between 1% and 25% of the radar center frequency, the signal is generally considered to be a wideband signal [10].

This article has been accepted for publication in a future issue of this journal, but has not been fully edited. Content may change prior to final publication. Citation information: DOI 10.1109/ACCESS.2019.2892113, IEEE Access

constant false alarm rate (CFAR). In fact, the papers that introduce new signals with a noise-like waveform have to optimize the matched filter to accommodate the new waveform shape.

4) Same processing gain as TC-OLA-based LFM radar system but with a higher spectrum spread, and therefore higher immunity to jamming.
5) Introduction of advanced synchronization modules to ensure a perfect recovery of the signal.
6) Possible implementation of the SSLFM TC-OLA radar using software-defined radar (SDR).

The remainder of this paper is structured as follows. Section II discusses the detail explanation and an analytical description of SSLFM TC-OLA radar. Section IV investigates the proposed radar under additive noise, and noise jamming. The validation of the theoretical model and its implementation in SDR is presented in Section V. We conclude and present our future work in Section VI.

II. Smeared Synthesized LFM TC-OLA radar

The block diagram of SSLFM TC-OLA radar is shown in Fig. 1, and depicts two ways to represent the proposed radar. Notice that, we use Table in our discussion. In the first way, the digitized LFM and the random phase signal are multiplied using Hadamard product, i.e. the element-wise product, to produce the synthesized LFM waveform (see path A, Fig. 1). In the second way, the signal is encoded by random phase during TC process (see path B, Fig. 1). The two ways of transmitting the radar signal have also two ways of reconstructing the signal at the receiver side. In what follows, the detail explanation including the analytical description of the transmitter, receiver, and synchronization systems.

TABLE I
Simulated parameters

General Radar Parameters	Symbol	Value	Units
Pulse Width	T_{pw}	100	μs
Pulse Repetition Interval	T_r	500	μs
Carrier Frequency	f_c	3	GHz
Coherent Pulse Interval	CPI	16	Scaler
LFM Radar Parameters	**Symbol**	**Value**	**Units**
Sampling frequency	f_{s_1}	2^{26}	MHz
Chirp bandwidth	B	15	MHz
TC-OLA-based LFM Radar Parameters	**Symbol**	**Value**	**Units**
Spreading factor	$\frac{M}{R}$	5	Scaler
Sampling frequency after TC	f_{s_2}	$\frac{M}{R} f_{s_1}$	MHz
Chirp bandwidth before spreading	B	15	MHz
Signal bandwidth after spreading	B_1	$\frac{M}{R} B = 75$	MHz
Wideband LFM Radar Parameters	**Symbol**	**Value**	**Units**
Sampling frequency	f_{s_2}	$\frac{M}{R} f_{s_1}$	MHz
Chirp bandwidth	B_1	$\frac{M}{R} B = 75$	MHz
SSLFM Radar Parameters	**Symbol**	**Value**	**Units**
Spreading factor	$\frac{M}{R}$	5	Scaler
Sampling frequency after TC	f_{s_2}	$\frac{M}{R} f_{s_1}$	MHz
Chirp bandwidth before spreading	B	15	MHz
Signal bandwidth after spreading	B_1	$\frac{M}{R} B = 75$	MHz
Noise factor	μ	1	Scaler
Target Parameters	**Symbol**	**Value**	**Units**
Target range	R_t	185.7	km
Target Doppler	f_d	7	kHz
CFAR type	CA-CFAR		
CFAR window size	W	8	Range cells
Probability of false alarm	P_{fa}	10^{-6}	-
Noise Parameters	**Symbol**	**Value**	**Units**
Noise type	Additive White Gaussian Noise (AWGN)		
Jamming Parameters	**Symbol**	**Value**	**Units**
Jamming type	Convolution noise jamming (CNJ)		
Jamming to Signal Ratio	JSR	35 and 40	dB

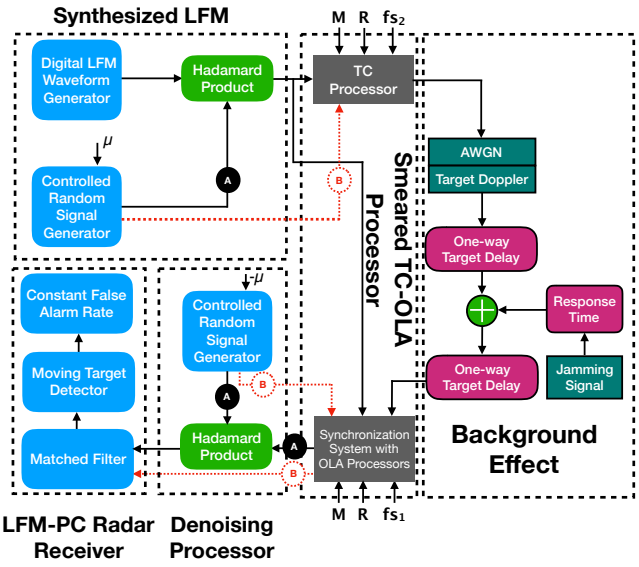

Fig. 1. Block diagram of SSLFM TC-OLA radar.

A. SSLFM TC-OLA Radar Transmitter

Let $x(n)$ be the digitized version of the LFM radar signal at sampling rate f_{s_1}, and L be the length of $x(n)$. Let $r(n)$ be a digital uniform random phase signal in $[0, 2\pi]$ of length L. The digital noise waveform $N(n)$ is defined as:

$$N(n) = e^{j\mu r(n)}, \forall n \in [0 \cdots L-1], \tag{1}$$

where μ is the noise factor. By increasing μ from 0 to 1, we produce a noise waveform with higher phase variation. As opposed to taking μ less than 0.5 as done in [5], we opted for $\mu = 1$ to get the full LPI advantage.

To noise the LFM signal, $x(n)$, we multiply it by the noise waveform, $N(n)$ as follows:

$$x_{syn}(n) = x(n)N(n). \tag{2}$$

The signal $x_{syn}(n)$ is the synthesized LFM (SLFM) signal. Fig. 2 shows the spectrogram of the LFM signal before and after product. The usual LFM spectrum occupies the chirp bandwidth B in the known linear shape while the SLFM spectrum is spread over the entire frequency bandwidth. Setting $\mu = 1$ renders $x_{syn}(n)$ a noise-like waveform. The signal after product is taken as reference signals in the receiver side.

Next, we apply the TC technique to $x_{syn}(n)$. The predefined parameters M, the segment length, and R, the hop size, are used to form the overlapping segments. The SLFM signal, $x_{syn}(n)$, is divided into overlapping sequences of segments $S_j, j \in [0, \frac{L-M}{R}]$, each S_j is a vector of length M defined as following the ideas in [6, 8]:

$$S_j = \Big[x_{syn}(jR), x_{syn}(1+jR), \ldots, x_{syn}(M-1+jR)\Big]. \tag{3}$$

Notice that the bound $\frac{L-M}{R}$ is not guaranteed to be integer unless M, L, and R are chosen in such a way to achieve that, or either by taking the lower or the higher integer of the term. Increasing the sampling frequency to $f_{s_2} = \frac{M}{R} f_{s_1}$, where f_{s_1} is the sampling frequency of the digitized LFM, produces a smeared synthesized signal with non-overlapping segments.

This article has been accepted for publication in a future issue of this journal, but has not been fully edited. Content may change prior to final publication. Citation information: DOI 10.1109/ACCESS.2019.2892113, IEEE Access

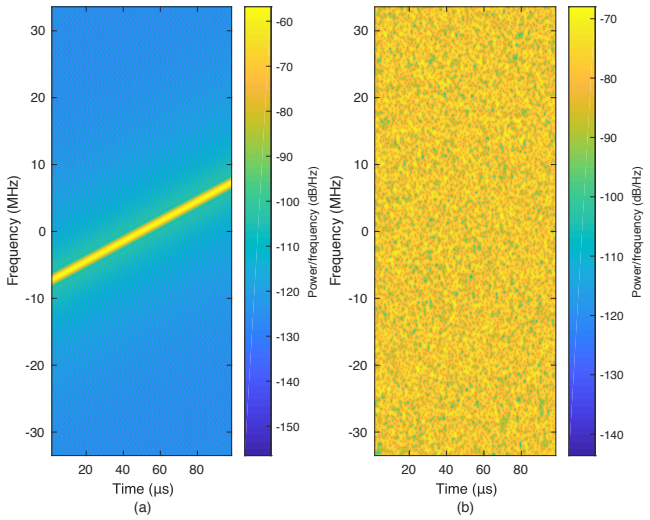

Fig. 2. (a) Spectrogram of LFM signal. (b) Synthesized LFM signal with $\mu = 1$.

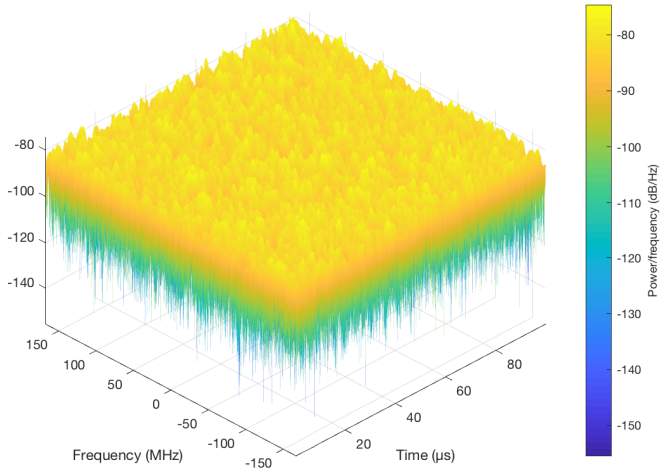

Fig. 3. Spectrogram of the SSLFM signal with $\frac{M}{R} = 5$ and $\mu = 1$.

The spectrum of the new signal is therefore spread by $\frac{M}{R}\frac{f_{s_1}}{B}$, where B is the radar bandwidth [8]. To express the transmitted signal, $x_t(n)$, a windowing function is introduced to select the proper segment via a shift. Since each segment overlaps with the next by $M-R$ samples, $n-i(M-R)$ gives the index of the transmitted value in the segment i. Therefore, the transmitted signal, $x_t(n)$ can be written as:

$$\begin{aligned} x_t(n) &= \sum_{i=0}^{L-M+1} w(n-iM)x_{syn}(n-i(M-R)) \\ &= \sum_{i=0}^{L-M+1} w(n-iM)x(n-i(M-R))N(n-i(M-R), \end{aligned} \tag{4}$$

where $w(n)$ is a windowing function that can be of any digital window function type [11]. The length of the windowing function, however, has to be $[0,\ldots,M-1]$. To cover only the finite length of the signal, the overlapping process should end at $L-M+1$. The expression of $x_t(n)$ is similar to the one we have in [8] except that each sample $x(n-i(M-R))$ is multiplied by $N(n-i(M-R))$. This allows the LFM TC signal to be smeared over the bandwidth $\frac{M}{R}f_{s_1}$. As such, $x_t(n)$ is called the *smeared SLFM TC* signal.

To preserve the time duration of the original signal $x(t)$, $x_t(n)$ is converted to continuous-time signal $x_t(t)$ by DAC at a high sampling rate $f_{s_2} = \frac{M}{R}f_{s_1}$. Fig. 3 shows how the TC processor smears the synthesized LFM signal over the bandwidth of $\frac{M}{R}f_{s_1}$. The power of the SSLFM signal is spread over the entire band instead of a restricted area as in TC-OLA-based LFM radar (see [8], Fig.6).

In addition to the target time delay, the signal is subjected to the channel effect including noise and the target Doppler shift. The result can be written as:

$$x_{t_c}(t) = x_t(t-t_d)e^{j2\pi f_d(t-t_d)} + n_r(t), \tag{5}$$

where f_d is the target Doppler shift, t_d is the target time delay, and $n_r(t)$ is the radar additive white Gaussian noise (AWGN).

Convolution noise jamming (CNJ) is a smart noise jamming techniques [12, 13] that is proposed for jamming LFM radars [14, 15]. In the CNJ context, the jammer receives the radar signal and convolves it with random signals. Therefore, less power is required to effectively jam the radar signal compared to other kinds of noise jamming technique [16].

The intercepted SSLFM signal at a self screening jammer (SSJ), a unit carrying a jamming equipment for its own protection, located at a distance $R_j = R_t$ from the radar is given by [12]:

$$S_{rj}(t) = x_t(t-t_j), \tag{6}$$

where t_j is the time delay of the signal expressed as R_j/c. The convolution noise jamming signal is:

$$\begin{aligned} J(t) &= S_{rj}(t) \circledast n_j(t-t_0) \\ &= x_t(t-t_j) \circledast n_j(t-t_0), \end{aligned} \tag{7}$$

where $\circledast$ is the convolution operator, $J(t)$ is the pulsed jamming signal, $n_j(t)$ is the jamming noise, t_0 is the response time that takes to transmit the jamming signal. The received jamming signal by the radar is therefore:

$$\begin{aligned} x_j(t) &= J(t-t_j) \\ &= x_t(t-2t_j) \circledast n_j(t-t_j-t_0). \end{aligned} \tag{8}$$

In the frequency domain, the jamming spectrum is multiplied by that of the signal and, therefore, noises the signal spectrum while keeping the spectral envelop the same. As such, the effect of jamming depends on the bandwidth of the signal and, in fact, decreases as the bandwidth of the signal increases. Under the same average jamming power, and since the SSLFM spectrum is spread over the entire $\frac{M}{R}f_{s_1}$ bandwidth, the effect of CNJ is significantly decreased compared to the standard or wideband LFM with B or $\frac{M}{R}B$ bandwidth, respectively. Moreover, the noise-like spectrum of the SSLFM signal makes it much better than the TC-OLA-based LFM as it has a higher LPI nature. Fig. 4 shows the effect of the CNJ on the wideband and TC-OLA-based LFM, and SSLFM signals. The standard LFM signal is not shown as it is a scaled version of the wideband LFM. As we can see,

This article has been accepted for publication in a future issue of this journal, but has not been fully edited. Content may change prior to final publication. Citation information: DOI 10.1109/ACCESS.2019.2892113, IEEE Access

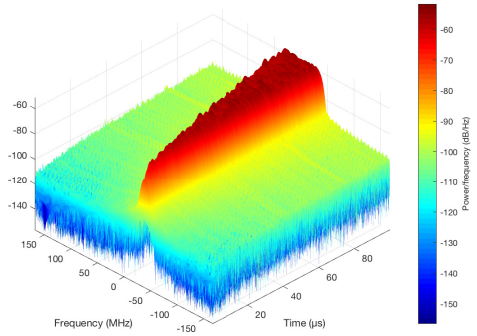

(a)

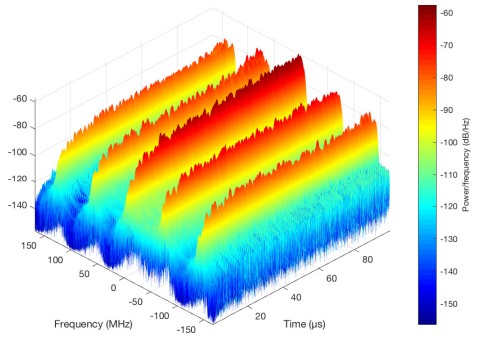

(b)

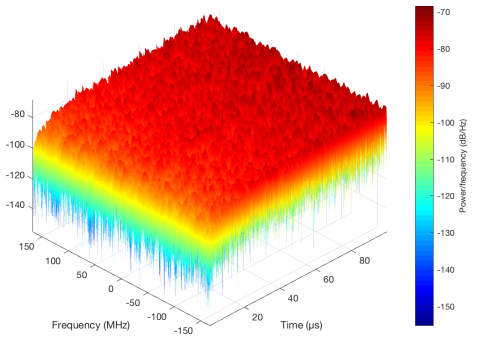

(c)

Fig. 4. Spectrogram of CNJ effect on: (a) wideband LFM signal with bandwidth $\frac{M}{R}B$, (b) TC-OLA-based LFM signal with $\frac{M}{R} = 5$, (c) SSLFM signal with $\frac{M}{R} = 5$.

the jamming noise spreads its power over the bandwidths of the signals.

Given the expression of $x_j(t)$, the total received signal can be formulated from Eq. 5 and Eq. 8 as follows:

$$x_r(t) = x_t(t - t_d)e^{j2\pi f_d(t-t_d)} + n_r(t) + x_j(t). \tag{9}$$

We rewrite the received signal as:

$$x_r(t) = X_t(t) + n_r(t) + x_j(t), \tag{10}$$

where $X_t(t) = x_t(t - t_d)e^{j2\pi f_d(t-t_d)}$ is the SSLFM signal that holds the target information.

B. SSLFM TC-OLA Radar Receiver

The received signal $x_r(t)$ is sampled via ADC at the sampling rate f_{s_2} to obtain a discrete-time signal $x_r(n)$. A synchronization system right after ADC is necessary to properly recover the signal at the OLA and denoising processors. Our proposed synchronization systems are discussed in the next subsection. For simplicity, we assume that the signal $x_r(n)$ is already synchronized and is fed to the OLA processor. This processor is then deployed to partition $x_r(n)$ into consecutive segments of length M; each segment is then shifted to the right by R with respect to its preceding segment and added to produce the synthesized LFM signal, $x_s(n)$. The shifting is carried out using the windowing function w to produce overlapping segments similar to the ones at the transmitter side. For a segment i and given that now the segments overlap over $M - R$, $n + i(M - R)$ gives the index of the value of x corresponding to the index n of the signal x_s. Therefore, $x_s(n)$ can be expressed as:

$$x_s(n) = \sum_{i=0}^{L-M+1} w(n - iR)x_r(n + i(M - R)). \tag{11}$$

We can rewrite $x_s(n)$ as:

$$x_s(n) = X_{t_{OLA}}(n) + N_{OLA}(n) + X_{j_{OLA}}(n), \tag{12}$$

where $X_{t_{OLA}}(n)$ is the OLA output of the SSLFM signal, $N_{OLA}(n)$ is the OLA output of AWGN, and $X_{j_{OLA}}(n)$ is the OLA output of jamming signal whose value depends on the jamming to signal ratio (JSR).

As shown in [8], the gain of the OLA output $X_{t_{OLA}}(n)$ increases by a factor of $(\frac{M}{R})^2$ while still preserving target information.

It is worth emphasizing that all processors coming after OLA carry out their operations at a lower sampling rate, f_{s_1}. The OLA processor is followed by the denoising processor. The denoising processor is used to remove the random noise phase from the signal by multiplying each sample of the signal by the conjugate of the corresponding random phase sample to produce the LFM signal, $x_f(n)$, as follows:

$$\begin{aligned} x_f(n) &= x_s(n)N^*(n) \\ &= x_s(n)e^{-j\mu r(n)}, \end{aligned} \tag{13}$$

where " $*$ " is the conjugate operator. Using Eq. 12, the reconstructed LFM signal can be written as:

$$x_f(n) = (X_{t_{OLA}} + N_{OLA} + X_{j_{OLA}})e^{-j\mu r(n)} \tag{14}$$

We can deduce from the previous equation that, with a good SS, the LFM signal is recovered while the jamming signal effect at the MF and MTD is reduced as a result of the element-wise multiplication by the conjugate of the random waveform. The output of the denoising process goes through the tradition LFM-PC radar receiver to detect the information of the target (time delay and Doppler shift). Namely, MF, MTD, and CFAR. MF is for maximizing SNR at its output [17, 18], MTD is for producing a 2-D array with rows corresponding to the Doppler cells and columns corresponding to the range cells [8], and CFAR is for computing the adaptive threshold at each Doppler

This article has been accepted for publication in a future issue of this journal, but has not been fully edited. Content may change prior to final publication. Citation information: DOI 10.1109/ACCESS.2019.2892113, IEEE Access

cell to maintain the certain value of a false alarm rate, P_{fa} [19, 20].

Comparing the proposed radar with the traditional LFM and TC-OLA-based LFM radar, we obviously see the superiority of our system over the others as shown in Fig. 5. As we move from the traditional LFM to the wide LFM, the processing gain increased by $\frac{M}{R}$ (5 in this case) as a result of the bandwidth increase. The receiver output of the TC-OLA-based LFM radar is almost the same as that of the wideband LFM radar [8]. The interesting aspect of SSLFM is that it kept the same TC-OLA-based LFM processing gain while it significantly reduced the effect of CNJ. In fact, the denoising did not only allow us to extract LFM from SLFM but also to cause CNJ to be very uncorrelated with the reference signal.

C. Synchronization System of SSLFM TCOLA Radar

The SS for the new proposed radar is of extreme importance as we are dealing with random phase signal. Deciding the beginning of the first segment is critical to produce the proper overlapping segments so that they can be added constructively.

Table II presents the list of symbols for easy addressing the explanation of our proposed SSs.

TABLE II
LIST OF SYMBOLS

Symbol	Description	Appear
MF	Impulse response of LFM signal	The conventional radar
$MF^{(1)}$	Impulse response of smeared LFM signal	SS#1 and SS#2
$MF^{(2)}$	Impulse response of smeared LFM signal (Low rate)	SS#2 and SS#3
x_i	Transmitted or reference signal in samples in case of path A - Fig. 1	Eq. 16
x'_i	Received Signal in samples in case of path A - Fig. 1	Eq. 18
x^f_i	Transmitted/reference signal in case of path B - Fig. 1	Eq. 37
$x^{f'}_i$	Received signal in case of path B - Fig. 1	Eq. 39

Given that the returned signal is formed from overlapping segments, each of length M, there are $M-1$ possible choices to select the first sample. As a consequence, we have to design a SS that is able to find the correct choice and reconstruct the incoming signal properly. For that, we propose three SSs. The first and second SSs target the first way, while the third SS targets the second way.

1) Synchronization System #1*:* Fig. 6 shows the first SS (SS#1). The SS involves M paths as shown in Fig. 6; each path contains three cascaded blocks, namely delay, OLA processor, and MF, denoted by $\text{MF}^{(1)}$. Let $\alpha : \{\alpha \in \mathbb{N} | 0 \leq \alpha \leq M-1\}$ be the shift value as well as the path number (e.g. if $\alpha = 0$, it corresponds to the first path). The received signal after OLA processor can be formulated as follows:

$$x_s^{\alpha}(n) = \sum_{i=0}^{L-M+1} w(n - iR) x_r(n + i(M-R) - \alpha) \qquad (15)$$

Although OLA is computed for all possible α shifts, only one will produce the correct OLA output. To illustrate this step, let the synthesized LFM signal be

$$x_{syn}(n) = [x_0 \; x_1 \; x_2 \; x_3 \; x_4 \; x_5 \; \ldots \; x_{L-1}], \qquad (16)$$

and let $M = 4$ and $R = 2$. Therefore the SSLFM signal is

$$x_t(n) = [x_0 \; x_1 \; x_2 \; x_3 \; x_2 \; x_3 \; x_4 \; x_5 \; x_4 \; x_5 \; \ldots \; x_{L-1}]. \qquad (17)$$

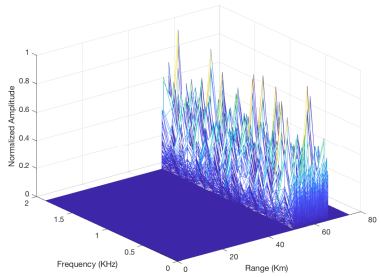

(a)

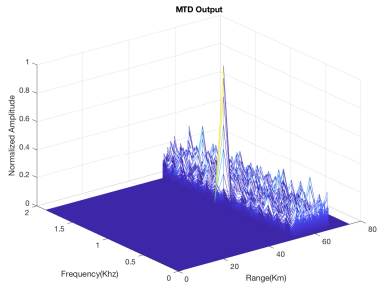

(b)

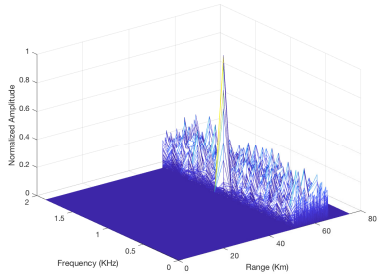

(c)

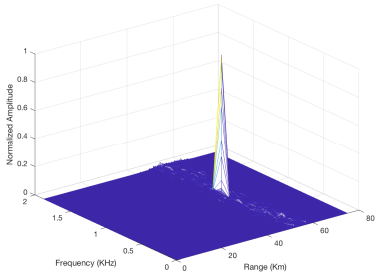

(d)

Fig. 5. The response of: (a) the traditional LFM radar, (b) the wideband LFM radar $5B$, (c) the TC-OLA-based LFM-PC radar, $\frac{M}{R} = 5$, (d) the SSLFM TC-OLA radar, $\frac{M}{R} = 5$, under JSR = 35 dB.

Notice that, the number of sample increases by amount of $\frac{M}{R}$. Assume that the incoming signal is delayed 2 samples:

$$x_r(n) = [0 \; 0 \; x'_0 \; x'_1 \; x'_2 \; x'_3 \; x'_2 \; x'_3 \; x'_4 \; x'_5 \; \ldots \; x'_{L-1}], \qquad (18)$$

where the samples x'_i include all the background effects. Although all the samples have different values, the samples with the same notations are expected to be added together by the OLA processor. At the first path, $\alpha = 0$, the OLA carries out its operation without shift. It means that the first

This article has been accepted for publication in a future issue of this journal, but has not been fully edited. Content may change prior to final publication. Citation information: DOI 10.1109/ACCESS.2019.2892113, IEEE Access

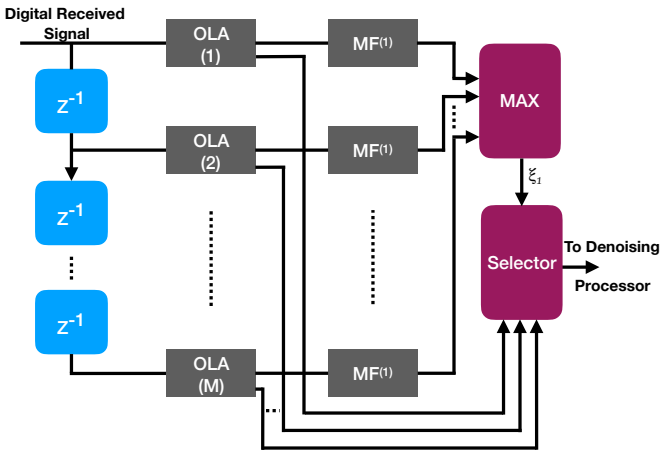

Fig. 6. Block diagram of SS#1 for TC-OLA processor.

segment $S_0 = [0\ 0\ x'_0\ x'_1]$ is added to the second segment $S_1 = [x'_2\ x'_3\ x'_2\ x'_3]$ after hopping by 2 samples and is also added to the third segment $S_3 = [x'_4\ x'_5\ x'_4\ x'_5]$ after hopping by 2 samples with respect to the second segment and so on. In particular, x'_0 and x'_1 in the first segment are added to x'_2 and x'_3 in the second segment, respectively. In the same way, x'_2 and x'_3 (sample number three and four) in the second segment are added to x'_4 and x'_5 (sample number one and two) in the third segment. As the result, the OLA processor gives the inappropriate signal.The two peaks are a consequence of the reference signal being half correlated with the overlapped signal. The second path deals with the received signal with one sample shift. In this case, the first three segments are $S_0 = [0\ 0\ 0\ x'_0]$, $S_1 = [x'_1\ x'_2\ x'_3\ x'_2]$, and $S_3 = [x'_3\ x'_4\ x'_5\ x'_4]$. Therefore, 0 and x'_0 in the first segment are added to x'_1 and x'_2 in the second segment, respectively. Also, x'_3 and x'_2 in the second segment are added to x'_3 and x'_4 in the third segment. One sample out of four is correctly added after each hop. Next, the OLA processor in the third path executes its operation after two sample shifts. The first three segments are $S_0 = [0\ 0\ 0\ 0]$, $S_1 = [x'_0\ x'_1\ x'_2\ x'_3]$, and $S_3 = [x'_2\ x'_3\ x'_4\ x'_5]$. The two zeros in the first segment are added to x'_0 and x'_1; x'_2 and x'_3 in the second segment are added to x'_2 and x'_3 in the third segment. The output of OLA in such case is properly overlapped. The last path output with three sample shifts is the same as the second path output as only one sample is correctly overlapped in each segment.

To search for the maximum peak, each OLA has to be followed by MF ($MF^{(1)}$); the impulse response of the MF is obtained by time-reversing and conjugating the synthesized LFM waveform $x_{syn}(n)$ as expressed below:

$$x^{\alpha}_{MF}(n) = \sum_{k=-\infty}^{\infty} x^{\alpha}_{s}(k) x^{*}_{syn}(T_{pw} + k - n), \tag{19}$$

where T_{pw} is the pulse duration that is added for the impulse response to be causal.

From Eq. 19, x^{α}_{s} and x^{*}_{syn} should be a matched pair to maximize the SNR output. If the OLA process changes the waveform (as in paths 1, 2, 4), a mismatch occurs and, in turn, a reduction of the correlation peak is observed. Fig. 7 shows the $MF^{(1)}$ output of each path after applying successive shifts before OLA processor.

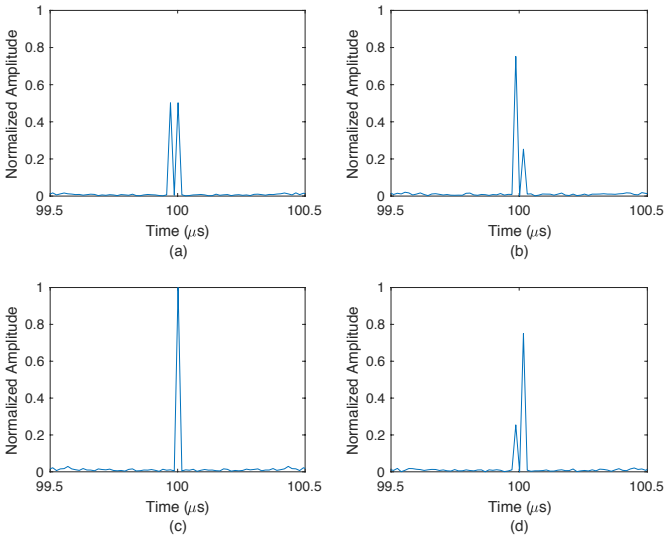

Fig. 7. Output of $MF^{(1)}$ for $M = 4$ and $R = 2$, and with (a) no shift, (b) one sample shift, (c) two sample shift, and (d) three sample shift.

Comparing the peaks at the output of $MFs^{(1)}$, we can detect the path number, ξ_1, for which the maximum correlation occurs. This path number can be written as the maximum of the maximum peaks as follows:

$$\xi_1 = \underset{SS_1}{\text{argmax}}\{\max(x^{SS_1}_{MF^{(1)}}(n))\}, \tag{20}$$

where $SS_1 : \{SS_1 \in \mathbb{N} | 0 \leq SS_1 \leq M-1\}$. The proper OLA output is selected according to ξ_1 value, and the output of SS#1 is:

$$x_s(n) = x^{\xi_1}_{s}(n). \tag{21}$$

In SS#1, we need $(M-1)$ unit delays, M OLA processors, and M MFs. This makes the implementation challenging for large M. For that reason, we offer a second SS, SS#2 as explained next.

2) Synchronization System #2: Fig. 8 shows the SS#2 which is composed of two multirate stages.

The first stage involves downsampling the received signal by a factor of M:

$$x_d(n) = x_r(nM). \tag{22}$$

Let $\beta : \{\beta \in \mathbb{N} | 0 \leq \beta \leq R-1\}$ The β shifted the R downsampled SLFM signal is given by:

$$x^{\beta}_{syn_d}(n) = x_{syn}(nR + \beta). \tag{23}$$

The R signals produced ($x^{\beta}_{syn_d}(n)$) are used to create the R-impulse responses, $h^{\beta}_{MF^{(2)}}(n)$, accordingly:

$$\begin{aligned} h^{\beta}_{MF^{(2)}}(n) &= x^{*\beta}_{syn_d}(T_{pw} - n) \\ &= x^{*}_{syn}(T_{pw} - (nR + \beta)) \end{aligned} \tag{24}$$

This article has been accepted for publication in a future issue of this journal, but has not been fully edited. Content may change prior to final publication. Citation information: DOI 10.1109/ACCESS.2019.2892113, IEEE Access

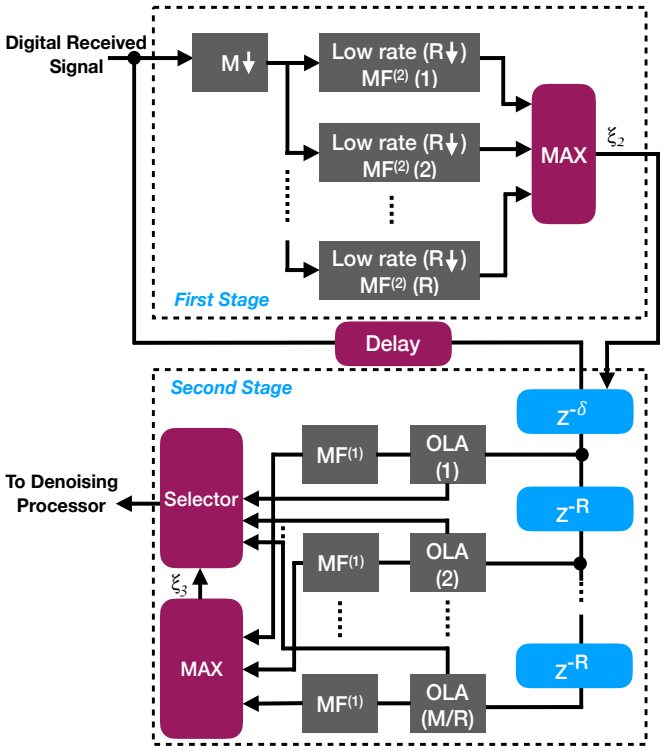

Fig. 8. Block diagram of SS#2 for TC-OLA processor.

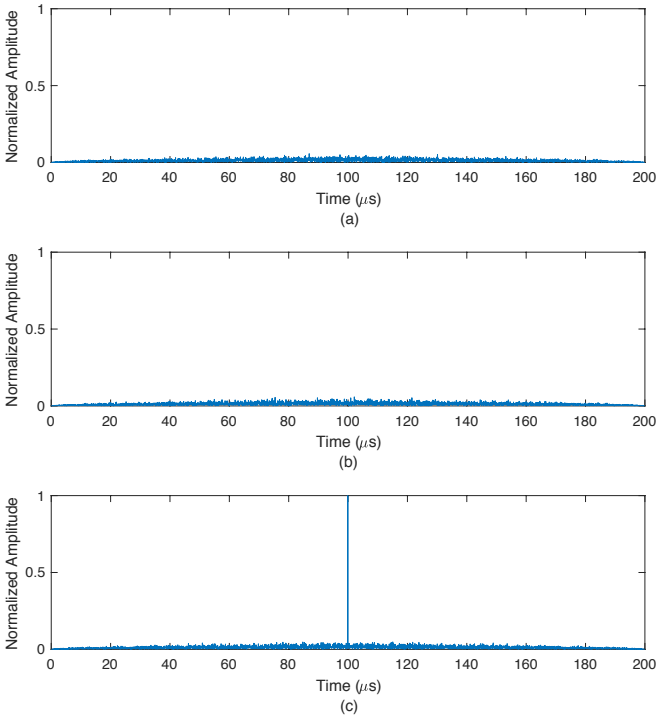

Fig. 9. The correlation output of $MF^{(2)}$, $M = 6$, $R = 3$, for: (a) $h^0_{MF^{(2)}}(n)$, (b) $h^1_{MF^{(2)}}(n)$, (c) $h^2_{MF^{(2)}}(n)$. Only the MF with the coefficients $x^2_{syn_d}(n)$ has an apparent correlation peak while the rest do not.

Using Eq. 22 and Eq. 24, the output of R-matched filters are:

$$x^{\beta}_{MF^{(2)}}(n) = \sum_{k=-\infty}^{\infty} x_r(kM) x^*_{syn}(T_{pw} + k - (nR + \beta)) \quad (25)$$

Only one filter is matched with the $x_d(n)$ and produces one peak. The other matched filters do not actually have any common samples with the incoming signal, which gives a very low correlation. For example, Let $M = 6$ and $R = 3$. Using the $x_{syn}(n)$ in Subsection II-C1, we have three versions of $x^{\beta}_{syn_d}(n)$ where β is 0, 1 and 2:

$$x^{\beta}_{syn_d}(n) = [x_\beta \;\; x_{R+\beta} \;\; x_{2R+\beta} \;\; x_{3R+\beta} \;\; x_{\frac{1}{R}(L-M+1)+\beta}] \quad (26)$$

The SSLFM signal is given by:

$$x_t(n) = [x_0 \; x_1 \; x_2 \; x_3 \; x_4 \; x_5 \; x_3 \; x_4 \; x_5 \; x_6 \; \ldots \; x_{L-1}].$$

Assume that the incoming signal is delayed 4 samples as follows:

$$x_r(n) = [0 \; 0 \; 0 \; 0 \; x'_0 \; x'_1 \; x'_2 \; x'_3 \; x'_4 \; x'_5 \; x'_3 \; x'_4 \; \ldots \; x'_{L-1}].$$

The incoming signal is then downsampled by a factor of 6 to be:

$$x_d(n) = [0 \; x'_2 \; x'_5 \; x'_8 \; \ldots \; x'_{\frac{1}{M}(L-1)}].$$

As we can see, the number of the missing samples, as a result of downsampling process, is $(R-1)$ and $x_d(n)$ has the same length as $x^{\beta}_{syn_d}(n)$.

Correlating $x_d(n)$ with all $h^{\beta}_{MF^{(2)}}(n)$ for $\beta = 0, 1, 2$, we found that $h^2_{MF^{(2)}}(n)$ produces the maximum correlation peak while the rest do not have any apparent peaks as shown in Fig. 9.

Similar to the first SS, the index of the matched filter which has a good correlation is given by:

$$\xi_2 = \underset{SS_2}{\text{argmax}}\{\max(x^{SS_2}_{MF^{(2)}}(n))\}, \quad (27)$$

where $SS_2 : \{SS_2 \in \mathbb{N} | 0 \le SS_2 \le R-1\}$. The shift value of the delay unit, δ, at the beginning of the second stage, is given by $\delta = \xi_2 - 1$.

In the second stage, the total number of delay units is $\frac{M}{R}$. The output of each delay unit is connected to the OLA processor. Let $\gamma : \{\gamma \in \mathbb{N} | 0 \le \gamma \le \frac{M}{R} - 1\}$, representing the index of each path in the second stage and, therefore, the shift value of the delay unit in each path (see Fig. 8). The output of the OLA, $x^{\gamma}_s(n)$, can be written as follows:

$$x^{\gamma}_s(n) = \sum_{i=0}^{N-M+1} w(n - iR) x_r(n + i(M-R) - (\delta + \gamma R)) \quad (28)$$

Back to the example above, the shift value of the first delay unit is 2 and is added to $x_r(n)$ before the OLA. At the first path, the first three segments at the output of OLA processor will be, $S_0 = [0 \; 0 \; 0 \; 0 \; 0 \; 0]$, $S_1 = [x'_0 \; x'_1 \; x'_2 \; x'_3 \; x'_4 \; x'_5]$, and $S_2 = [x'_3 \; x'_4 \; x'_5 \; x'_6 \; x'_7 \; x'_8]$. With hop size $R = 3$, the OLA gives the correct output. The OLA of the second path carries out its function after 5 samples delay. Therefore, the first three segments at the output of OLA processor are $S_0 = [0 \; 0 \; 0 \; 0 \; 0 \; 0]$, $S_1 = [0 \; 0 \; 0 \; x'_0 \; x'_1 \; x'_2]$, and $S_2 = [x'_3 \; x'_4 \; x'_5 \; x'_3 \; x'_4 \; x'_5]$. In this case, x'_0, x'_1, and x'_2 in the second segment are added to the

This article has been accepted for publication in a future issue of this journal, but has not been fully edited. Content may change prior to final publication. Citation information: DOI 10.1109/ACCESS.2019.2892113, IEEE Access

x_3', x_4', and x_5' in the third segment, and, therefore, produced the wrong output. Next, $MF^{(1)}$ is applied to each OLA output:

$$x^{\gamma}_{MF^{(1)}}(n) = \sum_{k=-\infty}^{\infty} x_s^{\gamma}(k) x^*_{syn}(T_{pw} + k - n) \tag{29}$$

From Fig. 10 and the above analysis, it is clear that the first matched filter has a good correlation compared to the second one. By detecting the peak, we obtain the index of the

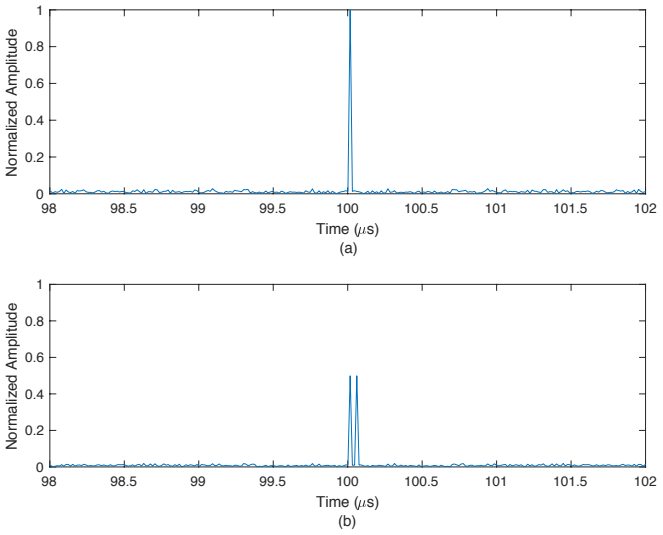

Fig. 10. The correlation output of $MF^{(1)}$ in the second stage - path A, with $M = 6$ and $R = 3$, for (a) 2 sample shifts, (b) 5 sample shifts.

appropriate path as follows:

$$\xi_3 = \underset{SS_3}{\text{argmax}}\{\max(x^{SS_3}_{MF^{(2)}}(n))\}, \tag{30}$$

where $SS_3 : \{SS_3 \in \mathbb{N} | 0 \leq SS_3 \leq \frac{M}{R} - 1\}$. Finally, the output of SS#2 is:

$$x_s(n) = x_s^{\xi_3}(n). \tag{31}$$

In SS#2, we need $\frac{M}{R}$ unit delays, $\frac{M}{R}$ OLA processors, and $\frac{M}{R}$ $MF^{(1)}$s and R $MF^{(2)}$s. For large M and $R > 1$, the complexity of the second approach is remarkably reduced compared to the first one. However, the computational complexity of OLA modules are relatively high. Therefore, we introduce a third SS, SS#3 to reduce the complexity of the previous SSs.

3) Synchronization System #3: This system targets the second way of the proposed radar (see Fig. 1, path *B*). Fig. 11 shows SS#3. Similar to SS#2, it consists of two multirate stages.

Since the noise phase is inserted during the TC process, the transmitted SSLFM signal, represented in Eq. 4, is now modified to:

$$x_t(n) = \sum_{i=0}^{L-M+1} w(n - iM) x(n - i(M - R)) N(n). \tag{32}$$

The length of $N(n)$ is now equal to the length of $x_t(n)$. In the first stage, the incoming signal is downsampled by a factor of M (See Eq. 22). One way to create the impulse response of MFs is from SSLFM signal (TC signal). Let $\beta' : \{\beta' \in \mathbb{N} | 0 \leq \beta' \leq M - 1\}$. The SSLFM signal downsampled by M and shifted by β' is given by:

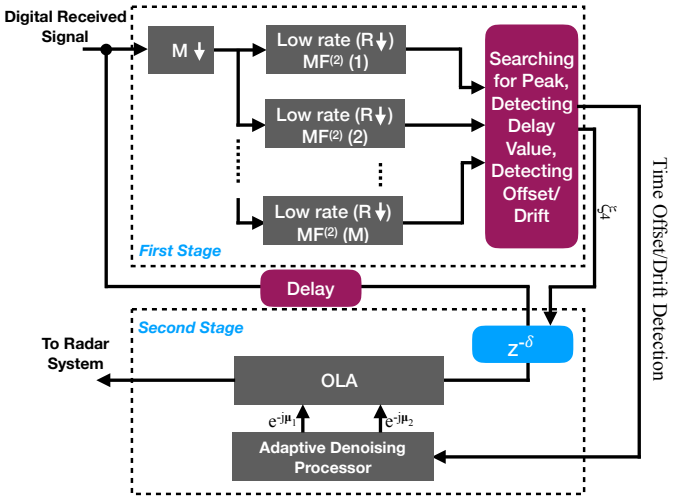

Fig. 11. Block diagram of SS#3 for TC-OLA processor.

$$x^{\beta'}_{syn_d}(n) = x_t(nM + \beta). \tag{33}$$

The M-impulse responses can be written as:

$$\begin{aligned} h^{\beta'}_{MF^{(2)}}(n) &= x^{*\beta'}_{syn_d}(T_{pw} - n) \\ &= x_t^*(T_{pw} - (nM + \beta')) \end{aligned} \tag{34}$$

Using Eq. 22 and Eq. 34, the output of M-matched filters are:

$$x^{\beta'}_{MF^{(2)}}(n) = \sum_{k=-\infty}^{\infty} x_r(kM) x_t^*(T_{pw} + k - (nM + \beta')) \tag{35}$$

Only one MF is matched with the $x_d(n)$ and gives one peak, while the others MFs do not have any common samples with the incoming signal, given thereby very low correlations. The index of the matched filter which has a maximum correlation is given by:

$$\xi_4 = \underset{SS_1}{\text{argmax}}\{\max(x^{SS_1}_{MF^{(2)}}(n))\}. \tag{36}$$

The shift value of the delay unit is given by $\delta = \xi_4 - 1$. To illustrate this, let us look at the example where M is 6 and R is 3. The SSLFM signal is given by:

$$x_t(n) = \left[x_0^0\ x_1^1\ x_2^2\ x_3^3\ x_4^4\ x_5^5\ x_3^6\ x_4^7\ x_5^8\ x_6^9 \ldots\ x_{L-1}^{\frac{M}{R}(L-1)}\right]. \tag{37}$$

Notice that the above equation is different from the Eq. II-C2 in SS#2. Each M segment is multiplied by M independent random phases. In other words, the random phase sample that is multiplied by x_4 in the first segment, for example, is different than the one that is multiplied by x_4 in the second segment.

Therefore, the six versions of $x^{\beta'}_{syn_d}(n)$, for $\beta' = 0, 1, \ldots, 5$:

$$x^{\beta'}_{syn_d}(n) = \left[x^{\beta'}_{\beta'}\ x^{\beta'+M}_{\beta'+R}\ x^{\beta'+2M}_{\beta'+2R} \ldots\ x^{(L-M+1)+\beta'}_{\frac{1}{R}(L-M+1)+\beta'}\right] \tag{38}$$

Assume that the incoming signal SSLFM is delayed by 3 samples:

This article has been accepted for publication in a future issue of this journal, but has not been fully edited. Content may change prior to final publication. Citation information: DOI 10.1109/ACCESS.2019.2892113, IEEE Access

$$x_t(n) = \left[0\ 0\ 0\ x_0^{0'}\ x_1^{1'}\ x_2^{2'}\ x_3^{3'}\ x_4^{4'}\ x_5^{5'}\ x_3^{6'}\ \dots\ x_{L-1}^{\frac{M}{R}(L-1)}\right]. \quad (39)$$

The incoming signal is then downsampled by a factor of 6 to be:

$$x_d(n) = \left[0\ x_3^{4'}\ x_6^{10'}\ x_9^{16'}\ \dots\ x^{\frac{1}{R}(L-1)}_{\frac{1}{M}(L-1)}\right]. \quad (40)$$

From Eq.40, $x_d(n)$ has the same length as $x^{\beta'}_{syn_d}(n)$. Correlating $x_d(n)$ with all $h^{\beta'}_{MF^{(2)}}(n)$ for $\beta' = 0, 1, \dots, 5$, it is easy to see the $h^3_{MF^{(2)}}(n)$ produces the maximum correlation peak while others do not as shown in Fig. 12. The shift value is

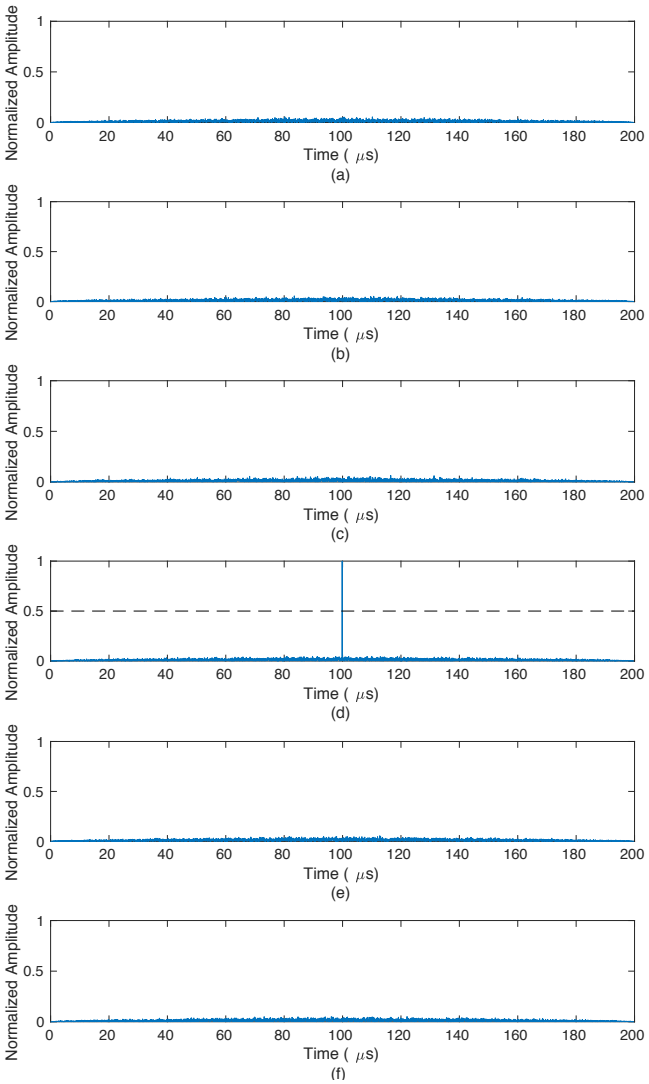

Fig. 12. The correlation output of $MF^{(2)}$ in the second stage - path B, $M = 6$, $R = 3$, for: (a) $h^0_{MF^{(2)}}(n)$, (b) $h^1_{MF^{(2)}}(n)$, (c) $h^2_{MF^{(2)}}(n)$, (d) $h^3_{MF^{(2)}}(n)$, (e) $h^4_{MF^{(2)}}(n)$, (f) $h^5_{MF^{(2)}}(n)$, Only the MF with the coefficients $x^3_{syn_d}(n)$ has an apparent correlation peak while the rest do not.

calculated as in Eq. 27. Unlike SS#2 that need extra work for reconstruction to be done, this shift value is directly used to determine the first sample and reconstruct the incoming signal properly.

The decision of time offset, the actual sampling time is out of sync by a consistent amount from the nominal sampling time throughout the system, or time drift, the actual sampling time is progressively out of sync over time from the nominal sampling time, is taken based on the output of MFs. Each MF output is divided by the maximum normalized correlation and the result is compared to a certain threshold, η, as follows:

$$\frac{x^{\beta'}_{MF^{(2)}}(n)}{\max\{\max(x^{(0)'}_{MF^{(2)}}(n)), \dots, \max(x^{(M-1)'}_{MF^{(2)}}(n))\})} \geq \eta, \quad (41)$$

where $\beta' = 0, \dots, M-1$. If two of them exceed the threshold, the decision goes to adaptive denoising processor to change its mode. In the drift/offset mode, the phase noise is interpolated using an upsampler followed by a low-pass filter:

$$\begin{aligned} N_{up}(nL) &= N(n) \\ N_{intp}(n) &= \sum_{k=0}^{k=N_{tap}-1} h_{lp}(k) N_{up}(n-k), \end{aligned} \quad (42)$$

where N_{up} is upsampled phase noise, N_{intp} is interpolated phase noise, and h_{lp} is the impulse response of the low-pass filter. After that, the downsampler picks the samples that are closely matched to the current state. Therefore, the adaptive random phase signal, N_{adapt} can be written as:

$$N_{adapt} = N(nM - \rho), \quad (43)$$

where ρ is the controlled time offset $\in [0, \frac{T_s}{2}]$.

The output of the OLA and also the output of SS#3 can be written as follows:

$$x_s(n) = \sum_{i=0}^{N-M+1} w(n - iR) x_r(n + i(M-R) - \delta) N^*(n). \quad (44)$$

Fig. 13 shows the problem of time offset of $0.45T_s$. The threshold is set to be 0.5 of the maximum correlation. Fig. 14

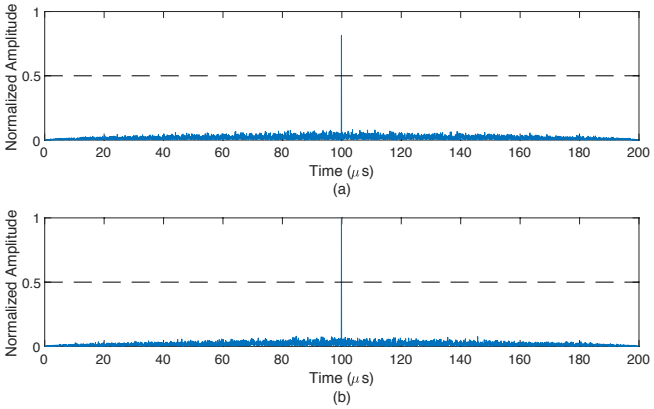

Fig. 13. Time offset problem of $0.45T_s$, $M = 6$, $R = 3$, and $\eta = 0.5$.

shows the output and OLA and denoising processors with and without the time offset correction. ρ is set to be $0.4T_s$. A notable enhancement in recovering signal is recorded. Notice that the recovered signal has extra gain of 2 as $\frac{M}{R} = 2$.

In *SS*#3, although we have increased the number of MFs, we need one unit delay, one OLA processor, and M $MF^{(2)}$s;

This article has been accepted for publication in a future issue of this journal, but has not been fully edited. Content may change prior to final publication. Citation information: DOI 10.1109/ACCESS.2019.2892113, IEEE Access

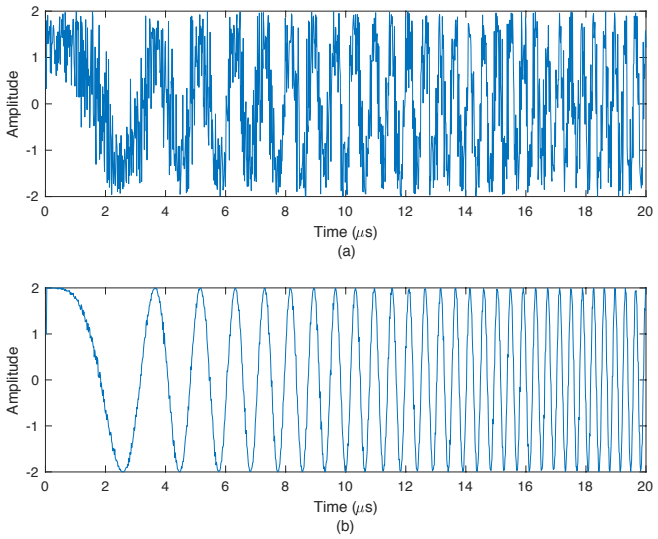

Fig. 14. The first 20μs of the output of the OLA and denoising processors, $\frac{M}{R} = 2$. (a) Without time offset correction, $\rho = 0$ (b) With time offset correction, $\rho = 0.4T_s$.

no need to add the MF after OLA processors as in SS#1 and SS#2. Therefore, the complexity of *SS*#3 depends mainly on M.

III. Analytical Description of SSLFM TC-OLA Radar

In this section, we rely on Table I to support our discussion.

A. SSLFM TC-OLA Synchronization System

In what follows, we elaborate on the three proposed SSs.

IV. Evaluation of SSLFM TC-OLA radar

In this section, the proposed radar is evaluated under AWGN and CNJ in the presence of moving target, and compared with the traditional LFM-PC radar, the TC-OLA LFM-PC radar, and a wideband LFM-PC radar having the same processing gain as our model. The parameters for these different radar systems is shown in Table I.

The evaluation is done using the Detection Probability Curve (DPC); such curve combines SNR with the probability of detection, P_D, under fixed probability of false alarm, P_{fa}. Notice that the SNR used in the simulation is calculated at the receiver front end.

A. Evaluation under AWGN

Fig. 15 shows the effect of the AWGN on the proposed radar compared to the other radars. The SSLFM processing gain is the same as the TC-OLA-based LFM and wideband LFM radars but 5 times (or 7 dB) greater than the traditional LFM radar because of the $\frac{M}{R}$ additional processing gain of OLA processor. From Fig. 15, the simulation result is consistent with our analytical result.

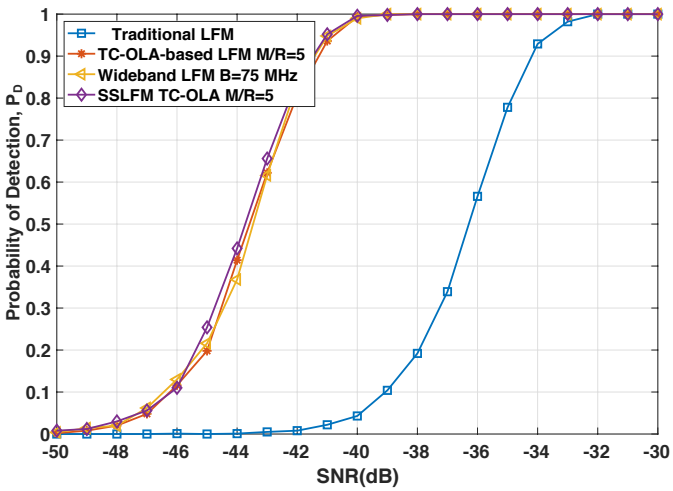

Fig. 15. DPC for traditional LFM, TC-OLA-based LFM, wideband LFM, and SSLFM TC-OLA radars under AWGN.

B. Evaluation under CNJ

The radar models are subjected to CNJ with a JSR of 35 dB. According to radar parameters, this value is chosen to totally jam the traditional LFM radar. With that JSR value the detection of TC-OLA-based LFM and wideband LFM radars is comparable to no jamming case. For example, in Fig. 15, TC-OLA-based LFM and wideband LFM radars achieve 100% in their detections at SNR = −40 dB. Fig. 16, with jamming, they achieve ≈ 58%, 72% in their detections, respectively. The

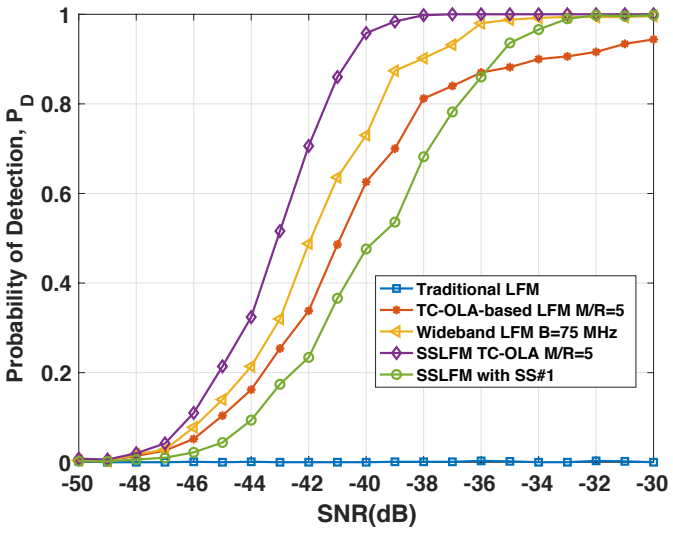

Fig. 16. DPC for traditional LFM, TC-OLA-based LFM, wideband LFM, and SSLFM TC-OLA radars under JSR = 35 dB.

SSLFM curve, shown in Fig. 16, has a very small degradation. In fact, at SNR = −40 dB, The radar has a detection of ≈ 98%.

To quantify the superiority of the proposed system, we increase JSR to 40 dB. Fig. 17 shows the performance of TC-OLA-based LFM, wideband LFM, and SSLFM TC-OLA radars.

The detection of the TC-OLA-based at SNR = −35 dB LFM radar is decreased to 20%, and that of the wideband LFM is below 50%. The SSLFM TC-OLA radar, however,

This article has been accepted for publication in a future issue of this journal, but has not been fully edited. Content may change prior to final publication. Citation information: DOI 10.1109/ACCESS.2019.2892113, IEEE Access

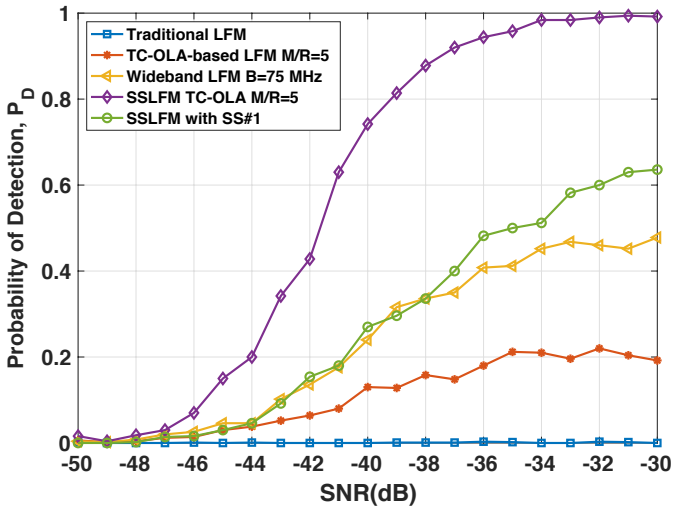

Fig. 17. DPC for TC-OLA-based LFM, wideband LFM, and SSLFM TC-OLA radars for JSR = 40 dB.

has detection almost 100% which is a huge improvement compared to the other radars. The green curves in both figures 16 and 17 will be discussed in Section IV-E.

C. Overall evaluation

From the above discussion, the SSLFM has better performance even under high noise jamming compared to TC-OLA-based LFM and wideband LFM. To take the comparison even further, we developed Table III for the reader to contrast the models from different aspects.

TABLE III
COMPARISON BETWEEN SSLFM TC-OLA, TC-OLA-BASED LFM, AND WIDEBAND LFM.

Aspects	SSLFM TC-OLA	TC-OLA-based LFM	Wideband LFM
Way of obtaining large bandwidth	Increasing the sampling frequency	Increasing the sampling frequency	Expanding the bandwidth
Radar resolution	Same as a traditional LFM radar	Same as a traditional LFM radar	Better (Increased by M/R)
Processing gain control	Easy (Change M and R parameters)	Easy (Change M and R parameters)	Fixed or replace the entire system
Spread spectrum control	Easy (Change M and R parameters)	Easy (Change M and R parameters)	Fixed or replace the entire system
Extra processing gain under AWGN	M/R (from TC and OLA processor)	M/R (from TC and OLA processor)	M/R (from bandwidth expansion)
Effect of CNJ under higher JSR (40 dB)	A very small degradation almost 0%	80% degradation	50% degradation
Design complexity	Low	Low	High
SDR implementation	Applicable according to maximum sampling rate	Applicable according to maximum sampling rate	Challenging (Sampling rate limitation and requires more resources)

In practice, the higher processing gain may not be achievable using a wideband LFM radar, since an existing LFM radar system will need to be redesigned to accommodate the new higher sampling rate. This may be straightforward in theory for a software-radio based radar system, but if the radar is a hardware-based design, such redesign may be costly or otherwise not practical in an operational context. Radar operations, in SSLFM and TC-OLA-based LFM, such as MF, MTD, and CFAR operate at the low sampling rate, thus enabling the use of more complex algorithms than that would be possible for a wideband LFM radar at the high sampling rate. The TC-OLA add-on does not require any modification or redesign of the existing LFM radar, which we see as a significant advantage.

Given that the SS is applied to the TC-OLA-based LFM and SSLFM TC-OLA, the latter includes a synthesized LFM and denoising modules in the transmitter and receiver, respectively (see Fig. 1). Although these modifications add extra complexity to the system, they are not costly as the added modules operate at a lower frequency. Furthermore, the overall system still has lower complexity compared to wideband LFM, and achieve higher immunity against noise jamming techniques compared to traditional LFM, wideband LFM, and TC-OLA-based LFM radars [8, 15, 21].

D. Evaluation of synchronization systems

We evaluate the three SSs in two ways. The first way looks at the statistical distributions of the errors at the selector output. while the second at the detection sensitivity of the overall system. Since SS#2 and *SS*#3 are done the synchronization in the same fashion, we suffice to evaluate SS#1 and SS#2. Both SSs are evaluated on a wide range of SNR for a few values of M and R.

1) Statistical performance: In this evaluation, pre-specified uniform distributed random delays $\in [0, \frac{T_s}{2}]$ are applied to the received signal and the computed delays based on the selector output is compared to the random delays for each SNR value from -40 dB to -20 dB. The probabilities of detection are gathered based on averaging 1000 of trials for each SNR value.

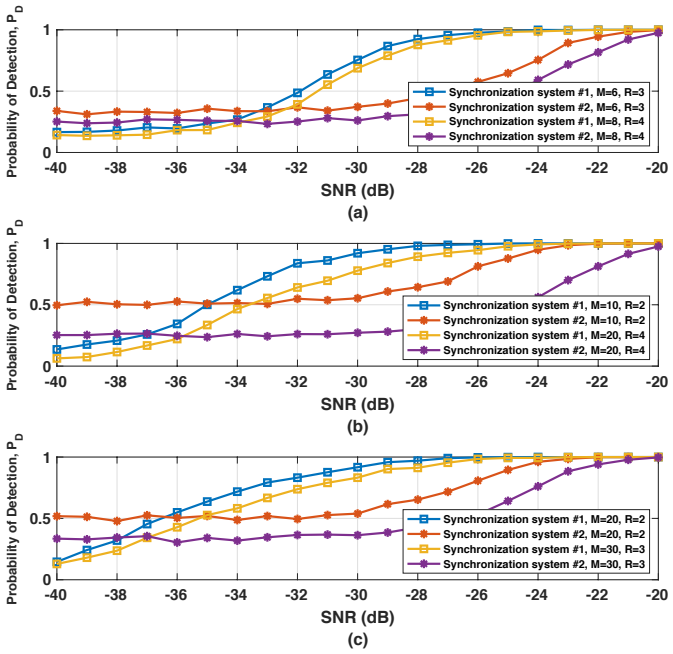

Fig. 18. Performance of the proposed synchronization systems. (a) $\frac{M}{R} = 2$, (b) $\frac{M}{R} = 5$, (c) $\frac{M}{R} = 10$.

Fig. 18 depicts the detection probabilities for different M and R values corresponding to $\frac{M}{R} = 2, 5$, and 10.

This article has been accepted for publication in a future issue of this journal, but has not been fully edited. Content may change prior to final publication. Citation information: DOI 10.1109/ACCESS.2019.2892113, IEEE Access

For SS#1, the detection probabilities are almost the same for a fixed $\frac{M}{R}$. To be precise, the performance is slightly less as the output of each OLA processor by nature exhibits some correlation with the MF in each path. Regardless of the path order, the maximum normalized amplitude, i.e. the amplitude of the peak, at the output of each path is approximately given by one of these values $\frac{1}{M}, \frac{2}{M}, \ldots, \frac{M-1}{M}, 1$. Thus, as M increases, the difference between the peaks becomes small, and, therefore, discriminating between the correct peak and the adjacent peaks becomes more sensitive to noise, causing P_D to be lower. This can be seen from Fig. 7 and Fig. 19 for $M = 8$ and $R = 4$. In fact, for $M = 4$ and $R = 2$, Fig. 7 shows 4 outputs for 4 paths. The amplitudes of the peaks are $\{0.25, 0.5, 0.75, 1\}$. Note that, the 0.25 output is accompanied with 0.75, Fig. 7(b) and (d), giving a complementary pair as a result of OLA property. Increasing M and R by 2, the set of the maximum normalized amplitudes becomes $\{0.125, 0.25, 0.3750, 0.5, 0.625, 0.75, 0.875, 1\}$ as shown in Fig. 19. Note that, the value 0.875 appears two times, Fig. 19 (b) and (h). Contaminating the received signal with noise will cause such a value to be very close to 1, and, therefore, increasing the difficulty to detect the correct output.

As $\frac{M}{R}$ increases the P_D increases as shown in Fig. 18. For instance, when $P_D = 0.5$, we have the following results:

1) $\frac{M}{R} = 2$, the SNRs are -32 and -31.5 dB for $\{M = 6, R = 3\}$ and $\{M = 8, R = 4\}$, respectively.
2) $\frac{M}{R} = 5$, the SNRs are -35 and -33.5 dB for $\{M = 10, R = 2\}$ and $\{M = 20, R = 4\}$, respectively.
3) $\frac{M}{R} = 10$, the SNRs are -36.5 and -35.5 dB for $\{M = 20, R = 2\}$ and $\{M = 30, R = 3\}$, respectively.

For SS#2, the P_D is dictated by the value of R, independently of $\frac{M}{R}$. As can be seen from Fig. 18(a), for $\frac{M}{R} = 2$ and $\{M = 8, R = 4\}$, the P_D curve is the same as the P_D curve in Fig. 18(b) corresponding to $\frac{M}{R} = 5$ and $\{M = 20, R = 4\}$. Likewise, the P_D curve in Fig. 18(a) for $\frac{M}{R} = 2$ and $\{M = 6, R = 3\}$, is the same as the P_D curve in Fig. 18(c) associated with $\frac{M}{R} = 10$ and $\{M = 30, R = 3\}$.

The dependency of P_D and R can be justified as follows. Given that the MFs of the first stage have a rate lower by R, the processing gain at the output of these low rate MFs are also lower by R. Therefore, as R increases, the processing gain becomes smaller and the low rate MFs become susceptible to noise. Although lowering the rate of MFs might look disadvantageous, it is very effective in producing uncorrelated signals in all paths except for the correct one (see Fig. 9).

2) Overall performance: The two SSs are followed by CFAR detectors to evaluate their overall performance and investigate their DPCs. It should be noticed that the CFAR detector was recomputed for each SS to satisfy a fixed P_{fa}, typically set to 10^{-6}. The same M and R values as in Subsection IV-D1 are also used here. Fig. 20 shows the DPCs for $\frac{M}{R} = 2, 5, 10$. The detection curve of the perfect synchronization case is used as the base line to which we compare the SSs detection curves.

For the two SSs, we can state the following:

- The detection performance is enhanced as $\frac{M}{R}$ increases.

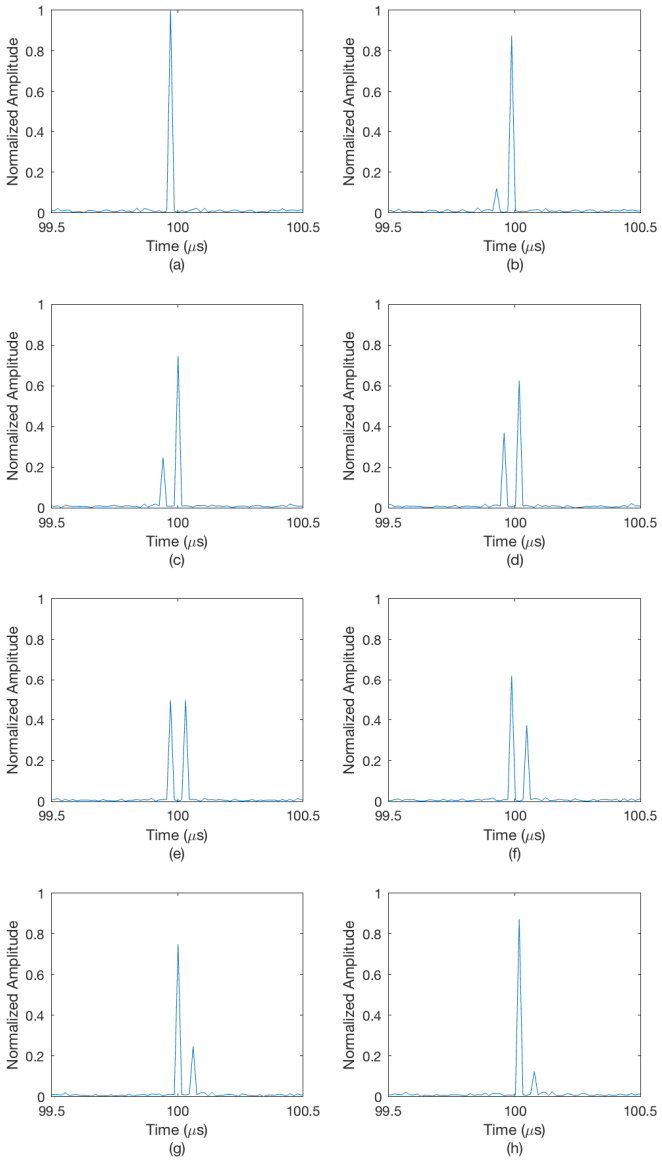

Fig. 19. Output of $MF^{(1)}$ for $M = 8$ and $R = 4$, and with (a) no shift, (b) one sample shift, (c) two sample shift, (d) three sample shift, (e) four sample shift, (f) five sample shift, (g) six sample shift, (h) seven sample shift, and (d) eight sample shift.

- As R increases, while keeping $\frac{M}{R}$ fixed, the P_d decreases for the same reason mentioned previously (see Subsection IV-D).
- As $\frac{M}{R}$ increases, the difference between the two PDCs increases as shown in Fig. 20(d).

Comparing the two SSs, it is clear that SS#1 is slightly better than SS#2. The SS#1 enhancement of the detection is not that much compared to its complexity with respect to SS#2. For example, for $M = 20$ and $R = 4$, SS#1 needs 20 OLA processors and 20 MFs while SS#2 only needs 4 low rate MFs, 5 OLA processors, and 5 normal rate MFs. This entails a 75% reduction in OLA processors and 55% in MFs.

This article has been accepted for publication in a future issue of this journal, but has not been fully edited. Content may change prior to final publication. Citation information: DOI 10.1109/ACCESS.2019.2892113, IEEE Access

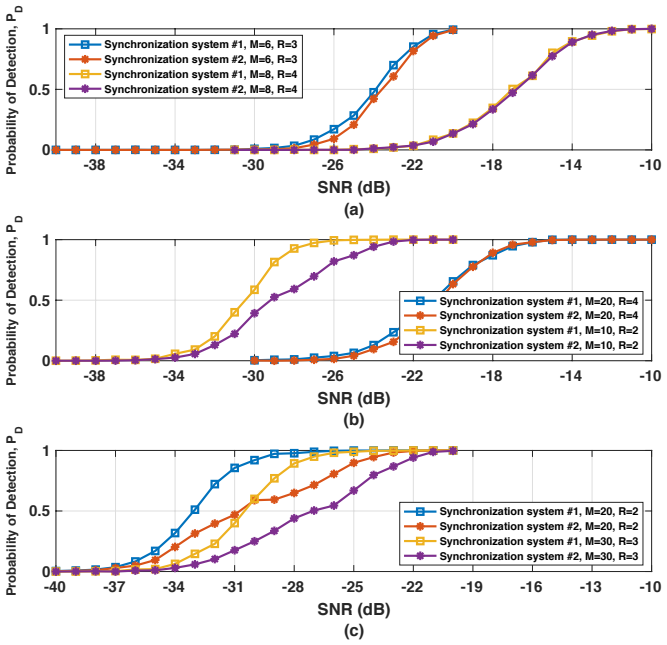

Fig. 20. Performance of the proposed synchronization systems. (a) $\frac{M}{R} = 2$, (b) $\frac{M}{R} = 5$, (c) $\frac{M}{R} = 10$.

E. Discussion

In the previous section, we investigated the performance of each SS as a standalone system. In this section, we will look at the performance of the entire system, after adding SS, to ensure the ongoing superiority of the proposed radar over the other radars. The performance of SSLFM TC-OLA radar with the SS#1 are shown in green in Fig. 16 and Fig. 17.

Under a JSR of 35 dB, from Fig. 16, at $P_D = 0.5$, the difference between the curves of the SSLFM TC-OLA with perfect synchronization and SSLFM TC-OLA with SS is $\approx$ 3 dB. As JSR increases to 40 dB, the SSLFM TC-OLA with SS reaches the limit of the SS performance and fails to provide reliable target detection. However, (See Fig. 17) the SSLFM TC-OLA with SS outperforms all the other radars except for the ideal SSLFM TC-OLA. As the figure shows, $P_D = 0.5$ is achieved at -41.5 dB and -36 dB for the ideal SSLFM TC-OLA radar and the SSLFM TC-OLA with SS, respectively. The wideband LFM radar has the same detection at -30 dB.

V. Hardware Proof of Concept

This Section introduces a proof of concept of our proposed synchronization systems. In this test, SS#3 has been selected. The entire radar system with different types of SSs is deferred to the next paper. Table IV presents the parameters used in the experiment. It should be noticed that the experiment is done by moving real data from MATLAB to GNU Radio and vice versa.

Fig. 21 shows the transmitted LFM signal (up-chirp) with time-frequency plot. This signal is time compressed and then transmitted through 960 ft coaxial cable to emulate the radar round trip. Fig. 22 shows the incoming signal. It is easy to see the spectrum of the received signal is spread over the entire band. Fig. 23 represents the first stage of *SS*#3. As

TABLE IV
Experimental Parameters

Parameters	Value	Units
SDR used	N210, PlutoSDR, and E310	
Sample frequency	5	MHz
Pulse Width	1	ms
LFM Bandwidth	1	MHz
Noise factor (μ)	1	Scaler
Segment length (M)	10	Scaler
Hop size (R)	2	scaler
TC sample frequency	6	MHz
Carrier Frequency	915	MHz

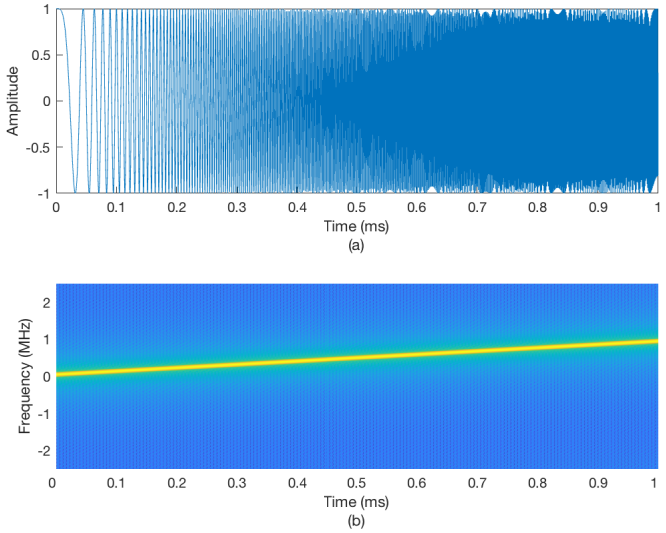

Fig. 21. (a) LFM signal, B=1MHz, (b) spectrogram of LFM signal.

we expected, there is no correlation between the MFs and the incoming signal except one. This indicates the shift value for the OLA and denoising processors. Fig. 24 represents the recovered LFM signal after OLAing and denoising the received signal. Comparing Fig. 22 with Fig. 24(b), *SS*#3 succeeded to recover the received signal.

VI. Conclusion and Future Work

We have presented a new radar system based on smearing the synthesized LFM signal using the TC-OLA technique. A new LPI signal with noise-like nature (using a high phase factor) is created while still possessing LFM features without changing in the standard LFM radar signal processing blocks. Although the proposed radar system has the same processing gain as TC-OLA-based LFM radar system, it enjoys a higher spectrum spread which increases the radar immunity against noise jamming techniques including CNJ. Moreover, the added modules (synthesizing and denoising at the transmitter and receiver respectively) operate at low frequency without increasing the complexity of the system while significantly improving the performance of detection.

Furthermore, three synchronization systems have been proposed for executing the overlap-add and the denoising processes properly. The limitation of the synchronization systems is mainly depending on the SNR and $\frac{M}{R}$ values as reported

This article has been accepted for publication in a future issue of this journal, but has not been fully edited. Content may change prior to final publication. Citation information: DOI 10.1109/ACCESS.2019.2892113, IEEE Access

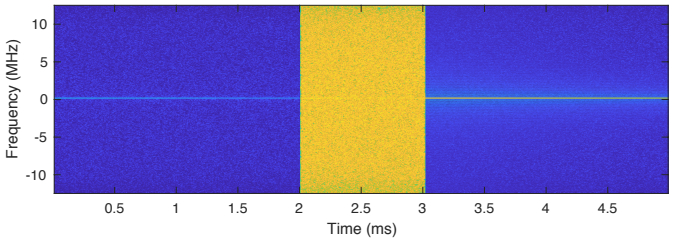

Fig. 22. Spectrogram of received SSLFM signal.

in Subsection IV-D. The SSLFM TC-OLA radar have been analyzed, simulated and then compared to traditional LFM, wideband LFM, and TC-OLA based LFM radars. The analysis shows that the new radar system is superior to the aforementioned radars. One of the SSs is evaluated experimentally using SDR. The result showed that it succeeded to recover the radar received signal. Currently, we are investigating the performance of the new system under other jamming and deception techniques.

Our future developments include further experimental evaluation of the proposed system using SDR, evaluating the system under different waveforms, such as phase coded waveforms and other frequency modulation waveform as we aim to build end to end radar system.

REFERENCES

[1] B. Li et al. “Waveform design for radar-embedded communications exploiting spread spectrum technology”. In: *IET Communications* 10.13 (2016), pp. 1631–1639.

[2] Y. Xiang et al. “A waveform with low intercept probability for OFDM SAR”. In: *Progress in Electromagnetic Research Symposium (PIERS)*. Aug. 2016, pp. 2054–2058.

[3] J. Chen, F. Wang, and J. Zhou. “Information content based optimal radar waveform design: LPI’s purpose”. In: *Entropy* 19.5 (May 2017), p. 210.

[4] M. A. Govoni, H. Li, and J. A. Kosinski. “Range-Doppler resolution of the linear-FM noise radar waveform”. In: *IEEE Trans. Aerosp. Electron. Syst.* 49.1 (2013), pp. 658–664.

[5] X. Feng et al. “Waveform design with low range sidelobe and high Doppler tolerance for cognitive radar”. In: *Signal Processing* 139 (Oct. 2017), pp. 143–155.

[6] S. Harrison and P. F. Driessen. “Novel UWB and spread spectrum system using time compression and overlap-add techniques”. In: *IEEE Access* 2 (2014), pp. 1092–1105.

[7] S. Harrison and P. F. Driessen. “Time compression overlap-add: Description and implementation”. In: *IEEE Pacific Rim Conference on Communications, Computers and Signal Processing (PACRIM)*. Aug. 2015, pp. 64–69.

[8] A. Youssef et al. “On time compression overlap-add technique in linear frequency modulation pulse compression radar systems: Design and performance evaluation”. In: *IEEE Access* 5 (2017), pp. 27525–27537.

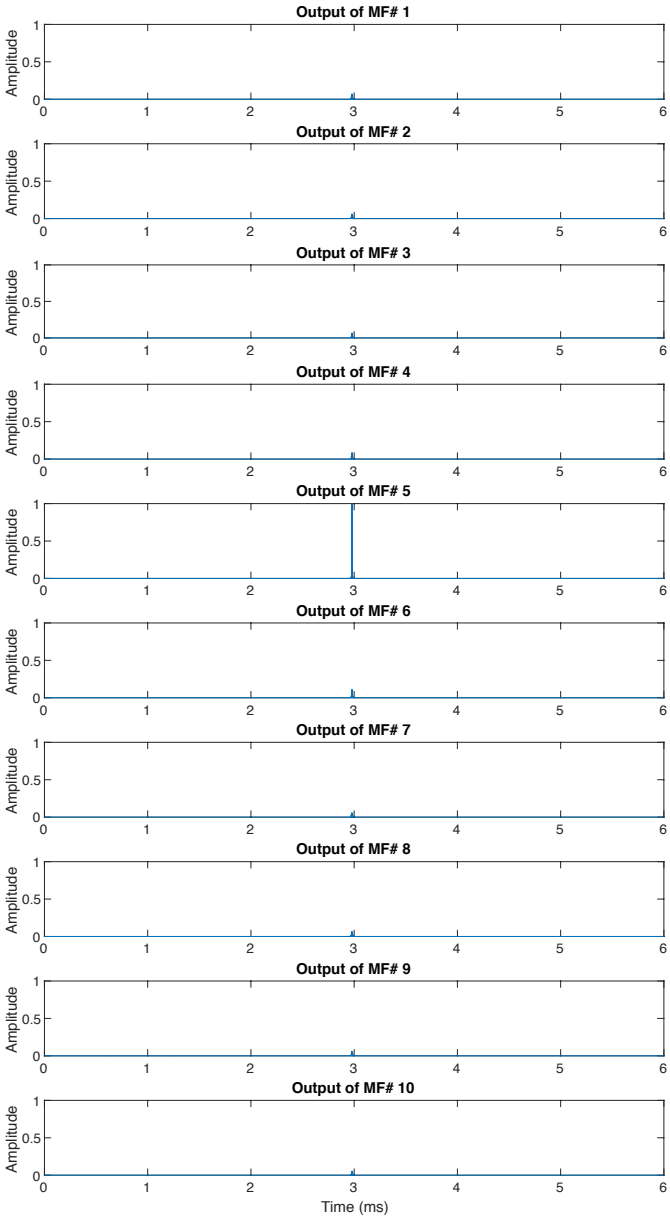

Fig. 23. Output of the synchronization system - stage 1. The received signal matches the MF number 5.

[9] A. Youssef et al. “Enhancement of time compression overlap-add using multirate downsample upsample shift add algorithm”. In: *IEEE Pacific Rim Conference on Communications, Computers and Signal Processing (PACRIM)*. Aug. 2017, pp. 1–5.

[10] M. A. Richards, J. A. Scheer, and W. A. Holm. *Principles of modern radar*. en. SciTech Publishing, Incorporated, May 2010.

[11] L. Tan and J. Jiang. *Digital signal processing: fundamentals and applications*. 2nd ed. Amsterdam; Boston: Elsevier/Academic Press, 2013.

[12] W. Ye et al. “Study of noise jamming based on convolution modulation to SAR”. In: *Computer, Mechatronics, Control and Electronic Engineering (CMCE),*

This article has been accepted for publication in a future issue of this journal, but has not been fully edited. Content may change prior to final publication. Citation information: DOI 10.1109/ACCESS.2019.2892113, IEEE Access

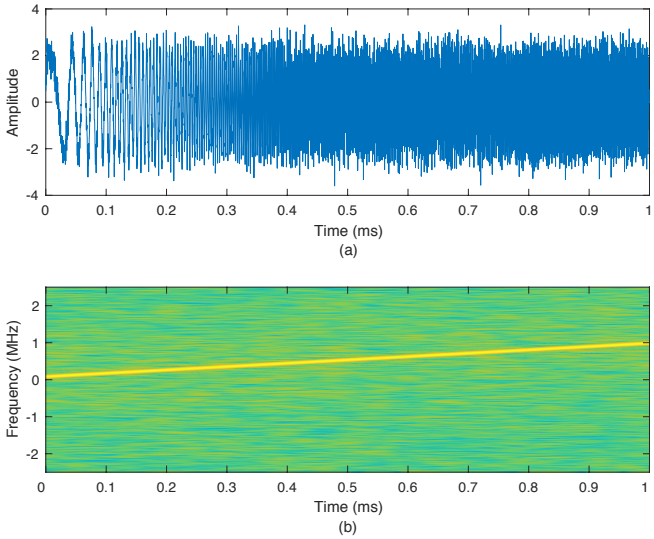

Fig. 24. Output of synchronization system - stage 2 after denoising and OLAing processes. (a) recovered LFM signal, (b) spectrogram of recovered LFM signal.

2010 International Conference on. Vol. 6. IEEE, 2010, pp. 169–172.

[13] J. Jiang, Y. Wu, and H. Wang. "Analysis of active noise jamming against synthetic aperture radar ground moving target indication". In: *8th International Congress on Image and Signal Processing (CISP)*. Oct. 2015, pp. 1530–1535.

[14] Z. Shao-quan and Y. Yang. "Convolution Jamming Technique Countering LFM Radar". In: *Journal of Electronics & Information Technology* 6 (2007), p. 030.

[15] A. Abouelfadl et al. "Performance analysis of LFM pulse compression radar under effect of convolution noise jamming". In: *Radio Science Conference (NRSC), 33rd National*. IEEE, 2016, pp. 282–289.

[16] H. Hu and N. Wei. "A study of GPS jamming and anti-jamming". In: *2nd International Conference on Power Electronics and Intelligent Transportation System (PEITS)*. Vol. 1. Dec. 2009, pp. 388–391.

[17] M. Skolnik. *Radar Handbook, Third Edition*. McGraw-Hill Education, 2008.

[18] B. R. Mahafza. *Radar Signal Analysis and Processing Using MATLAB*. CRC Press, 2016.

[19] M. I. Skolnik. *Introduction to Radar Systems*. Tata McGraw Hill, 2001.

[20] G. Galati. *Advanced Radar Techniques and Systems*. Peter Peregrinus, 1993.

[21] A. Youssef et al. "Performance evaluation of time compression overlap-add radar systems based on order-statistics CFAR under convolution noise jamming". In: *IEEE Pacific Rim Conference on Communications, Computers and Signal Processing (PACRIM)*. Aug. 2017, pp. 1–6.